Astron. Astrophys. 319, 1007–1019 (1997)

ASTRONOMY
AND
ASTROPHYSICS

Global evolution of solid matter in turbulent protoplanetary disks

II. Development of icy planetesimals

T.F. Stepinski[1] **and P. Valageas**[2]

[1] Lunar and Planetary Institute, 3600 Bay Area Blvd., Houston, TX 77058, USA
[2] Service de Physique Théorique, CEN Saclay, F-91191 Gif-sur-Yvette, France

Received 20 June 1996 / Accepted 12 September 1996

Abstract. It is currently thought that planets around solar-type stars form by the accumulation of solid matter entrained in a gaseous protoplanetary disk. We model part of this process starting from small particles suspended in a gaseous disk, and ending up with most of the solid material aggregated into 1–10–km–sized planetesimals. The radial distribution of solid material circumnavigating a star in the form of the planetesimal swarm is the major result of this study, inasmuch as it provides insight into the large-scale character of the emerging planetary system. The model simultaneously keeps track of the evolution of gas and solid particles due to gas-solid coupling, coagulation, sedimentation, and evaporation/condensation. For simplicity, we concentrate on solids made up solely of water–ice. We have found that the radial distribution of mass locked into planetesimals is sensitive to initial conditions. Two illustrative examples corresponding to two different initial conditions are presented: a high-mass, high-concentration case that starts with a disk of 0.24 $M_\odot$ extending up to 15 A.U. from the star, and a low-mass, low-concentration case that starts with a disk of 0.02 $M_\odot$ extending up to 250 A.U. from the star. The high-mass model leads to all solids being lost to the star; however, the low-mass model leads to a radial distribution of solid material quite reminiscent of what is found in our solar system.

Key words: accretion disks – solar system: formation

1. Introduction

Recently, with the identification of a solar-like star showing evidence for planets circling around it (Mayor & Queloz 1995), our interest in understanding the formation of a planetary system on its largest scale has intensified and widened beyond the long-standing question of the origin of the solar system. It is therefore timely to attempt, on theoretical grounds and from an evolutionary point of view, a prediction of the large-scale properties of a planetary system around a solar-like star. Of particular interest is the spatial distribution of material making up a planetary system, as this is about the only information the present observations, based on the Doppler technique, can provide. To start addressing this problem we are developing a model that would keep track of circumstellar material as it evolves from the form of a protoplanetary disk to the form of a planetary system. In the first paper of the series (Stepinski & Valageas 1996; hereafter referred to as Paper I) we laid down the foundations of our model and developed a numerical method to study the effects of aerodynamic forces acting on solid particles entrained in a gaseous disk. We refer the reader to that paper for elucidation of the essential concepts underlying our approach.

In the current paper we take our model one step further by taking into consideration the processes of coagulation, sedimentation, and evaporation/condensation of solid particles. These processes, acting in addition to gas-solid coupling caused by aerodynamic forces, shape the radial distribution of solid material around the star, until such time when solids augment to planetesimal sizes and further evolution of solid material is dominated by mutual gravitational interaction between planetesimals. Thus, our model, in its present form, given some initial distribution of gaseous and solid matter, computes the evolution of these two components, and can predict the radial distribution of solid mass locked into the planetesimal swarm. Arguably, such a distribution should well approximate the radial apportionment of condensed components of the planets spread over the radial extent of the mature planetary system. This is because the process of accumulation of planetesimals into planets or planetary cores is thought to happen with minimum radial displacement.

The location of solid mass in the present-day solar system presents an inevitable test for our model, and the bulk of our calculations were carried out to determine what kind of initial conditions, if any, lead to the development of a planetesimal swarm consistent with the solid matter in the solar system. Indeed, we have found initial conditions leading to a configuration of solid matter in rough agreement with the large-scale architecture of the solar system. However, we have also found that the outcome is sensitive to initial conditions, as well as, in some cases, to the values of the free parameters characterizing our model.

This opens the theoretical possibility of planetary system diversity. Additional diversity may result from the different quantities of gas that various planetary systems may subsequently add to some of their solid protoplanets. Note that, although we argue that our present model may predict the mass distribution of a condensed material in a nascent planetary system, it cannot predict the distribution of a whole planetary mass consisting of solid and volatile materials. Nevertheless, as solid protoplanets or cores constitute the backbone of a planetary system onto which volatile envelopes are subsequently added, modeling its structure is of a primary interest.

The major novelty of our work is its emphasis on the global, comprehensive treatment of the problem. This follows from our interest in attempting to establish the link between initial conditions that characterize a protoplanetary disk at the onset of star-disk formation, and the large-scale character of an ultimate planetary system. To achieve this goal we have to include all relevant physical processes. This, in turn, presented us technically and, to certain degree, conceptually with an intricate problem, which required major simplification in order to become tractable. Therefore, our handling of several processes, most notably coagulation, is less advanced than can be found in some published work (for a review see Weidenschilling & Cuzzi 1993) dedicated exclusively to the issue of coagulation and not addressing the evolution of solids globally. In order to make progress, we have assumed that the size distribution of particles at any given radial location of a disk is narrowly peaked about a mean value particular for this location and time instant. Such an approximation was first proposed by Morfill (1985). This allows us to keep track of the increase of the mean particle size alone, and frees us from daunting calculations required for computing the shift in the entire particle size distribution function. This approximation is important for the viability of our calculations. It also captures the essence of the coagulation process accurately enough, at least for our purpose, which is to keep track of solid's mass whereabouts regardless of how it is apportioned between particles of different sizes. Two other major simplifications characterize our current model. First, we concentrate on ice, the most abundant component of solid material, and disregard other compositional constituents such as "rock" and "metal." Hence, at present, we expect to model only the development of icy planetesimals, or outer zones of planetary systems. In the context of the solar system, we expect to model distribution of mass presently located in solid cores of giant planets. Second, unlike in the calculations by Cuzzi et al. (1993), which were devoted to the investigation of growth and sedimentation of solid particles at the *fixed* radial location, we assume that the evolution of the gaseous component remains unaffected by the changing character of the solid component. These last two assumptions provide the current model with much desired amenability; however, unlike the assumption about coagulation, they could be removed without jeopardizing the integrity of our method.

Our basic method of simultaneously keeping track of the evolution of gaseous and solid components of protoplanetary disks is described in Sect. 2. Separately, in Sect. 3, we describe our treatment of coagulation and evaporation processes, and offer a very brief depiction of our numerical technique. The next two sections are devoted to the presentation of results. In Sect. 4 the results for an initially high-mass, high-concentration disk are given, and in Sect. 5 an initially low-mass, low-concentration disk is examined for various values of dimensionless viscosiameter α. Finally, in Sect. 6, we present discussion and conclusions.

2. Basic design of our model

The evolution of both the gas and solid particles is described by equations of continuity

$$\frac{\partial}{\partial t}\rho + \nabla \cdot (\rho \mathbf{V}) = 0 \tag{1}$$

and momentum conservation

$$\frac{\partial}{\partial t}(\rho \mathbf{V}) + \nabla \cdot (\rho \mathbf{V}\mathbf{V}) = -\nabla P - \rho \nabla \Phi - \rho \frac{\mathbf{v}}{\mathbf{t}_{\rm s}} \tag{2}$$

Terms associated with external sources of mass are absent in these equations, as we restrict ourselves to considering only a dissipative stage of a protoplanetary disk. Note that the equation of momentum conservation is written in its conservative form. The preference for the conservative form over the more familiar force form [which can be easily obtained by combining (2) and (1)] will become clear momentarily. Both the gas and solid particles are considered to be perfect fluids. Thus, for the gas, P is simply the thermodynamic pressure, but for the particles $P = 0$. The last term on the right-hand side of (2) represents frictional coupling between particles and the gas. It is neglected in the computation of gas evolution, but preserved in the computation of particle behavior. We neglect the disk's self-gravity and assume that despite the growing mass of the central star its gravitational potential Φ remains constant. The symbol $\mathbf{VV}$ denotes the dyadic product of two velocity vectors.

The gas is explicitly assumed to be turbulent; thus quantities such as gas and particle velocities and densities are broken up into average and fluctuating parts

$$\rho = \overline{\rho} + \rho' \quad \text{and} \quad \mathbf{V} = \overline{\mathbf{V}} + \mathbf{V}' \tag{3}$$

Fluctuations of the gas are conveyed to particles by frictional coupling.

Cylindrical polar coordinates $(r,\ \phi,\ z)$ are used, and an axial symmetry ($\partial/\partial\phi = 0$) is assumed throughout the paper. The basic procedure is identical for both the gas and the particles; representation (3) is substituted into Eq. (2), which is then expanded out and the Reynolds averaging technique is applied to isolate the relationship between average quantities characterizing the state of the gas and the particles. The effects of turbulence manifest themselves by the presence of the correlation terms, $\overline{V_i' V_j'}$, $\overline{\rho' V_i'}$, and $\overline{\rho' V_i' V_j'}$ in the averaged equation. Note that because the averaging was applied to the equation of motion in the conservative form no correlation terms involving derivatives of fluctuating quantities appear. As there are no acknowledged models of such correlations, the preference for

using the conservative form of the equation of motion becomes evident. Nonvanishing correlations are modeled in terms of averaged quantities, and the equation of motion is solved under the thin disk approximation. The evolution of the mass in the disk is derived by vertically integrating the continuity equation (1) supplemented by the equation of motion.

In the remainder of this paper subscript d denotes quantities describing the state of solids, whereas quantities describing gas have no subscript.

2.1. Evolution of gas

Applying the procedure described above to the gaseous component of the disk we obtain

$$\frac{\partial}{\partial t}(\overline{\rho}\overline{\mathbf{V}}) + \nabla\cdot(\overline{\rho}\overline{\mathbf{V}}\,\overline{\mathbf{V}}) + \nabla\cdot\tau = -\nabla\overline{P} - \overline{\rho}\nabla\Phi \tag{4}$$

where τ is the stress tensor resulting from interactions among the fluctuations in the flow field

$$\tau_{ij} \stackrel{\rm def}{=} \overline{\rho}\,\overline{V_i'V_j'} + \overline{\rho' V_j'}\,\overline{V_i} \tag{5}$$

The presumption that $\rho' \ll \overline{\rho}$ makes it possible to neglect the triple correlations $\overline{\rho' V_i' V_j'}$ in definition (5). The remaining correlations $\overline{V_i'V_j'}$, $\overline{\rho' V_i'}$ are modeled in terms of averaged quantities. The diagonal components of the tensor $\overline{V_i'V_j'}$ are expressed in terms of a turbulent kinetic energy per unit mass

$$\overline{V_i'V_i'} = \frac{1}{3}V_{\rm t}^2 \tag{6}$$

The off–diagonal elements of the symmetric tensor $\overline{V_i'V_j'}$ are specified to mimic the corresponding elements of stress associated with molecular viscosity

$$\begin{aligned}
\overline{V_r'V_\phi'} &= -\nu_{\rm t} r\frac{\partial}{\partial r}\left(\frac{\overline{V_\phi}}{r}\right), \qquad \overline{V_z'V_\phi'} = -\nu_{\rm t}\left(\frac{\partial\overline{V_\phi}}{\partial z}\right)\\
\overline{V_r'V_z'} &= -\nu_{\rm t}\left(\frac{\partial\overline{V_z}}{\partial r} + \frac{\partial\overline{V_r}}{\partial z}\right)
\end{aligned} \tag{7}$$

Finally, the correlations of the form $\overline{\rho' V_i'}$ are modeled by the gradient diffusion hypothesis

$$\overline{\rho' V_r'} = -D\frac{\partial\overline{\rho}}{\partial r}, \qquad \overline{\rho' V_z'} = -D\frac{\partial\overline{\rho}}{\partial z}, \qquad \overline{\rho' V_\phi'} = 0 \tag{8}$$

Turbulent stress, τ, is characterized by three quantities, turbulent viscosity $\nu_{\rm t}$, turbulent diffusivity D, and turbulent velocity $V_{\rm t}$ given by

$$\nu_{\rm t} = \frac{1}{3}\alpha C_s H, \quad D = K\frac{1}{3}\alpha C_s H, \quad V_{\rm t} = \sqrt{2^{1/2}R_o\alpha}C_s \tag{9}$$

where H is the disk's vertical scale-height (used as a measure of the disk's thickness) and C_s is the speed of sound. The character of turbulence is encapsulated into three dimensionless parameters: the Shakura-Sunyaev dimensionless viscosity parameter α, the Rossby number for turbulent motions R_o, and K, which can be identified with the inverse of the turbulent Prandtl number. In our calculations we assume these parameters to be constant and uniform and use $K = 3$, $R_o = 3$, and α in the range from 10^{-4} to 10^{-1}. Note that in order for our model of τ [Eqs. (6) to (8)] to be self-consistent and physically meaningful, $R_o > 3/2$ is required. Otherwise, the Schwarz inequality applied to the Reynolds averaging operation is not satisfied, which leads to the averages of the square of some real fluctuating quantities to be negative. This detail is worth mentioning because models of τ, identical or similar to ours are often used, but rarely checked for consistency.

With such a model of turbulence and the stress tensor resulting from it, the self-consistent solution to Eq. (4) can be found under the thin disk ($H/r \ll 1$) approximation. The r-component of Eq. (4) determines the average tangential velocity $\overline{V_\phi}$. Under the assumption of vertical equilibrium ($\overline{\rho V_z} = 0$) and vertical isothermicity, the z-component of Eq. (4) yields the vertical profile of the disk's density and sets the scale-height, $H = \sqrt{2}C_s/\Omega_{\rm k}$, where $\Omega_{\rm k} = V_{\rm k}/r$ is the keplerian angular velocity. The average vertical velocity, $\overline{V_z}$, is obtained directly from the condition of vertical equilibrium. Finally, the ϕ-component of Eq. (4) gives the average radial velocity $\overline{V_r}$. Putting everything together, we have

$$\begin{aligned}
\overline{V_r} &= -\frac{3}{\overline{\rho}V_{\rm k}}\frac{1}{r}\frac{\partial}{\partial r}(r\overline{\rho}\nu_{\rm t}V_{\rm k}) + \frac{D}{\overline{\rho}}\frac{\partial\overline{\rho}}{\partial r} + \frac{\nu_{\rm t}}{r}\frac{\partial\ln T}{\partial\ln r}\left[1 - 2\frac{z^2}{H^2}\right]\\
\overline{V_\phi} &= V_{\rm k} + \frac{r}{2\overline{\rho}V_{\rm k}}\frac{\partial\overline{P}}{\partial r} - \frac{3}{4}V_{\rm k}\left(\frac{z}{r}\right)^2\\
\overline{V_z} &= -\frac{2D}{H^2}\,z
\end{aligned} \tag{10}$$

It's worth pointing out that $\overline{V_z} \neq 0$; even so vertical equilibrium is assumed. This is because the equilibrium requires the entire mass flux $\overline{\rho V_z} = \overline{\rho}\,\overline{V_z} + \overline{\rho' V_z'}$ to vanish, and $\overline{V_z}$ must be nonzero in order for $\overline{\rho}\overline{V_z}$ to balance $\overline{\rho' V_z'}$.

The Reynolds averaged continuity equation (1) is

$$\frac{\partial\overline{\rho}}{\partial t} + \frac{1}{r}\frac{\partial}{\partial r}(r\overline{\rho V_r}) + \frac{\partial}{\partial z}(\overline{\rho V_z}) = 0 \tag{11}$$

Integrating over the z coordinate and substituting $\overline{\rho V_r} = \overline{\rho}\,\overline{V_r} + \overline{\rho' V_r'}$ we obtain the familiar equation for time evolution of the surface density ($\Sigma = \int\overline{\rho}dz$) of the gas

$$\frac{\partial\Sigma}{\partial t} - \frac{3}{r}\frac{\partial}{\partial r}\left[r^{1/2}\frac{\partial}{\partial r}(r^{1/2}\nu_{\rm t}\Sigma)\right] = 0 \tag{12}$$

Notice that the last term on the left-hand side of Eq. (11) vanishes due to vertical integration, regardless of whether $\overline{\rho V_z}$ vanishes or not. Because $\nu_{\rm t}$ is not an explicit function of time, but instead depends only on the local disk's quantities [see Eq. 9)], it can be expressed as $\nu_{\rm t} = \nu_{\rm t}(\Sigma, r)$ and Eq. (12) can be solved subject to boundary conditions on the inner and outer edges of a disk and the opacity law. Given $\Sigma(r,t)$, we can algebraically find all other disk variables.

2.2. Evolution of solid particles

Applying the procedure described at the beginning of this section to the solid particle component of the disk we obtain

$$\frac{\partial}{\partial t}(\overline{\rho_{\rm d}\mathbf{V}_{\rm d}}) + \nabla\cdot(\overline{\rho_{\rm d}\mathbf{V}_{\rm d}}\,\overline{\mathbf{V}_{\rm d}}) + \nabla\cdot\tau_{\rm d} = -\overline{\rho_{\rm d}}\nabla\Phi - \overline{\rho_{\rm d}}\frac{\overline{\mathbf{v}}}{t_{s*}} \qquad (13)$$

where $\mathbf{v} = \mathbf{V}_{\rm d} - \mathbf{V}$ is the relative velocity between particles and the gas, and $t_{\rm s}$ is the stopping time. When averaging the gas-solids coupling term we approximate that $\overline{\rho_d\mathbf{v}/t_s} = \overline{\rho_d}\,\overline{\mathbf{v}}/t_{s*}$, where $t_{s*} = t_s(|\overline{\mathbf{v}}|)$ if $|\overline{\mathbf{v}}| > V_{\rm t}$ and $t_{s*} = t_s(V_{\rm t})$ if $|\overline{\mathbf{v}}| < V_{\rm t}$. The tensor $\tau_{\rm d}$ is given by

$$\tau_{ij\rm d} \stackrel{\rm def}{=} \overline{\rho_{\rm d}}\,\overline{V'_{i\rm d}V'_{j\rm d}} + \overline{\rho'_{\rm d}V'_{j\rm d}}\,\overline{V_{i\rm d}} \qquad (14)$$

where again, like in the case of the gas [see Eq. (5)], we have neglected the triple correlation $\overline{\rho'_{\rm d}V'_{i\rm d}V'_{j\rm d}}$ in definition (14). As we did in paper I, following the arguments given by Cuzzi et al. (1993) and Dubrulle et al. (1995), we model correlations $\overline{V'_{i\rm d}V'_{j\rm d}}$ as $\overline{V'_iV'_j}/{\rm Sc}$ and $\overline{\rho'_{\rm d}\mathbf{V}'_{\rm d}}$ as $-D/{\rm Sc}\ \nabla\overline{\rho_{\rm d}}$, where Sc denotes the Schmidt number

$${\rm Sc} = (1+\Omega_{\rm k}t_{s*})\sqrt{1+\frac{\overline{\mathbf{v}}^2}{V_{\rm t}^2}} \qquad (15)$$

We also define the quantities

$$\nu_{\rm td} = \frac{\nu_{\rm t}}{\rm Sc}, \quad D_{\rm d} = \frac{D}{\rm Sc}, \quad V_{\rm td}^2 = \frac{V_{\rm t}^2}{\rm Sc} \qquad (16)$$

The magnitude of the dimensionless quantity $\Omega_{\rm k}t_{s*}$ determines the aerodynamic regime. If $\Omega_{\rm k}t_{s*} \to 0$, the stopping time is small in comparison with the period of orbital revolution and particles are strongly coupled to the gas. This happens usually, but not exclusively, when particles are small, their size, s, smaller than about 1 mm. If $\Omega_{\rm k}t_{s*} \to \infty$, the stopping time is very long in comparison with the period of orbital revolution and particles are decoupled from the gas. This happens for large particles with $s > 10^4$ cm. The behavior of intermediate-sized particles is characterized by the $\Omega_{\rm k}t_{s*} \sim 1$ regime.

We seek a self-consistent solution to Eq. (13) under the thin disk approximation. Such a solution is required to be valid and self-consistent for all aerodynamic regimes. This cannot be achieved by the approximation fully analogical to the one we have used for the gas. Specifically, vertical transport of the r-component of momentum is not negligible in the $\Omega_{\rm k}t_{s*} \sim 1$ regime. However, as our primary goal is to calculate the global evolution of the mass residing in solid particles, we are not interested in details of solid material vertical distribution, with the sole exception of its scale-height. Therefore, instead of seeking a solution to Eq. (13) we can look for a solution to the system of equations consisting of the z-component of (13) and density-weighted vertical averages of r and ϕ components of (13). It turns out that the terms responsible for the vertical transport of the r-component of momentum vanish when averaged, and a self-consistent solution, valid for all aerodynamic regimes , can be found.

We start with the z-component of (13) and assume that particles are vertically in equilibrium so $\overline{\rho_{\rm d}V_{z\rm d}} = \overline{\rho_{\rm d}}\,\overline{V_{z\rm d}} + \overline{\rho'_{\rm d}V'_{z\rm d}} = 0$ or

$$\frac{\partial\overline{\rho_{\rm d}}}{\partial z} = \frac{1}{D_{\rm d}}\overline{\rho_{\rm d}}\,\overline{V_{z\rm d}} \qquad (17)$$

Because of vertical equilibrium, only two terms, both originating from $\nabla\cdot\tau_{\rm d}$, remain on the left-hand side of the z-component of (13). Of these we preserve a term containing $\tau_{zz\rm d}$ but neglect a term containing $\tau_{zr\rm d}$. We preserve all terms on the right-hand side of this equation. Using (17) and (10) we transform the z-component of (13) into

$$\overline{V_{z\rm d}}\left[\frac{1}{D_{\rm d}}\left(\frac{1}{3}{V_{\rm td}}^2 - \overline{V_{z\rm d}}^2\right) - 2\frac{\partial\overline{V_{z\rm d}}}{\partial z}\right] = -\ {\Omega_{\rm k}}^2 z - \frac{\overline{V_{z\rm d}}}{t_{s*}} - \frac{2D}{H^2 t_{s*}}z \qquad (18)$$

with $\overline{V_{z\rm d}}$ being the only unknown variable. In order to solve this equation we expand $\overline{V_{z\rm d}}$ in a Taylor series at $z = 0$

$$\overline{V_{z\rm d}} = -\frac{2D_{\rm d}}{H_{\rm d1}}\left(\frac{z}{H_{\rm d1}}\right) - \frac{4D_{\rm d}}{H_{\rm d3}}\left(\frac{z}{H_{\rm d3}}\right)^3 + \ldots \qquad (19)$$

The absence of even terms in expansion (19) follows from $\overline{V_{z\rm d}}$ being an odd function of z. Substituting this expansion into (17) and integrating the resulting equation we obtain the vertical profile of $\overline{\rho_{\rm d}}$

$$\overline{\rho_{\rm d}} = \overline{\rho_{\rm od}}\ \exp\left\{-\left(\frac{z}{H_{\rm d1}}\right)^2 - \left(\frac{z}{H_{\rm d3}}\right)^4 + \ldots\right\} \qquad (20)$$

It's clear that the characteristic length of a particle's vertical distribution is determined by quantities $H_{\rm di}$. Substituting (19) into (18) and comparing the terms proportional to z and z^3, respectively, we find $H_{\rm d1}$ and $H_{\rm d3}$ to be

$$\left(\frac{H_{\rm d1}}{H}\right)^2 = \frac{1}{2{\rm Sc}(1+\frac{3\Omega_{\rm k}t_{s*}}{\sqrt{2}K\alpha})}\times \left[A + \sqrt{A^2 + 8\Omega_{\rm k}t_{s*}(\Omega_{\rm k}t_{s*} + \frac{\sqrt{2}K\alpha}{3})}\right] \qquad (21)$$

where $A \stackrel{\rm def}{=} 1 + R_o\frac{\Omega_{\rm k}t_{s*}}{K}$, and

$$\left(\frac{H_{\rm d3}}{H}\right)^4 = \left(\frac{H_{\rm d1}}{H}\right)^6 \times \left[8\left(\frac{H}{H_{\rm d1}}\right)^2 + \frac{3\sqrt{2}R_o{\rm Sc}}{2{\rm K}^2\alpha} + \frac{3{\rm Sc}}{\sqrt{2}{\rm K}\alpha\Omega_{\rm k}{\rm t}_{s*}}\right] \qquad (22)$$

For particles in the $\Omega_{\rm k}t_{s*} \to 0$ regime, $H_{\rm d1} \to H$ and $H_{\rm d3} \to \infty$. The vertical distribution of solids and gas are the same, an expected result in the regime that stands for a perfect gas-solids coupling. For particles in the $\Omega_{\rm k}t_{s*} \sim 1$ regime, $H_{\rm d1} \sim$

$H_{\rm d3} \sim \sqrt{\alpha}H$, and for particles in the $\Omega_{\rm k}t_{\rm s*} \rightarrow \infty$ regime, $H_{\rm d1} \sim \sqrt{\alpha/{\rm Sc}}H$, whereas $H_{\rm d3} > H_{\rm d1}$. In all regimes we use $H_{\rm d1}$ as a measure of solid particles sub-disk thickness $H_{\rm d}$.

We now consider density-weighted, vertical averages of the r and ϕ components of Eq. (13). As our goal is to calculate the relative velocity between particles and gas, we also have to consider density-weighted, vertical averages of the r and ϕ components of the momentum conservation equation for the gas (4). Because the gas and particles have different vertical distributions of density we introduce two different averaging operators

$$\langle A \rangle \stackrel{\rm def}{=} \frac{\int_{-\infty}^{+\infty} \overline{\rho} A dz}{\Sigma} \quad \text{and} \quad \langle A \rangle_{\rm d} \stackrel{\rm def}{=} \frac{\int_{-\infty}^{+\infty} \overline{\rho_{\rm d}} A dz}{\Sigma_{\rm d}} \tag{23}$$

We apply the operator $\langle A \rangle_{\rm d}$ to components of (13), to get:

$$\langle \overline{v_\phi} \rangle_{\rm d} = V_{\rm k} - \langle \overline{V_\phi} \rangle_{\rm d} - \frac{3}{8} V_{\rm k} \left(\frac{H_{\rm d1}}{r} \right)^2 + \frac{\langle \overline{v_r} \rangle_{\rm d}}{2\Omega_{\rm k} t_{\rm s*}} \tag{24}$$

$$\begin{aligned} \langle \overline{v_r} \rangle_{\rm d} = & - \langle \overline{V_r} \rangle_{\rm d} - 3r^{-1/2} \frac{\partial}{\partial r}(r^{1/2}\nu_{\rm td}) \\ & + (D_{\rm d} - 3\nu_{\rm td}) \frac{1}{\Sigma_{\rm d}} \frac{\partial \Sigma_{\rm d}}{\partial r} - \frac{2\langle \overline{v_\phi} \rangle_{\rm d}}{\Omega_{\rm k} t_{\rm s*}} \end{aligned} \tag{25}$$

Now we have to evaluate $\langle \overline{\mathbf{V}} \rangle_{\rm d}$. When particles are small, in the $\Omega_{\rm k}t_{\rm s*} \rightarrow 0$ regime, $H_{\rm d1} \rightarrow H$ and $\overline{\rho_{\rm d}} \propto \overline{\rho}$, the dust is well mixed with the gas and $\langle \overline{\mathbf{V}} \rangle_{\rm d} = \langle \overline{\mathbf{V}} \rangle$. In this case,

$$\langle \overline{V_\phi} \rangle_{\rm d} = V_{\rm k} + \frac{1}{2\Omega_{\rm k}\Sigma} \frac{\partial}{\partial r} \left(C_s^2 \Sigma \right) - \frac{3}{8} V_{\rm k} \left(\frac{H}{r} \right)^2 \tag{26}$$

$$\langle \overline{V_r} \rangle_{\rm d} = -3r^{-1/2} \frac{\partial}{\partial r}(r^{1/2}\nu_{\rm t}) + (D - 3\nu_{\rm t}) \frac{1}{\Sigma} \frac{\partial \Sigma}{\partial r} \tag{27}$$

When particles are big, in the $\Omega_{\rm k}t_{\rm s*} \rightarrow \infty$ regime, $H_{\rm d1} \rightarrow 0$, the dust is concentrated in the midplane and $\langle \overline{\mathbf{V}} \rangle_{\rm d} \approx \overline{\mathbf{V}}(z = 0)$. Thus, in this regime we get:

$$\langle \overline{V_\phi} \rangle_{\rm d} = V_{\rm k} + \frac{1}{2\Omega_{\rm k}\rho_{\rm o}} \frac{\partial P_{\rm o}}{\partial r} \tag{28}$$

$$\begin{aligned} \langle \overline{V_r} \rangle_{\rm d} = & -3r^{-1/2} \frac{\partial}{\partial r}(r^{1/2}\nu_{\rm t}) + (D - 3\nu_{\rm t}) \frac{1}{\rho_{\rm o}} \frac{\partial \rho_{\rm o}}{\partial r} \\ & + \frac{\nu_{\rm t}}{r} \frac{\partial \ln T}{\partial \ln r} \end{aligned} \tag{29}$$

where the subscript o denotes the value of a vertically changing quantity evaluated at $z = 0$. For the intermediate-sized particles the values of $\langle \overline{V_\phi} \rangle_{\rm d}$ and $\langle \overline{V_r} \rangle_{\rm d}$ are somewhere midway between these given by Eqs. (26)-(27) and these given by Eqs. (28)-(29). Therefore, for all regimes we can use the following formulas

$$\begin{aligned} \langle \overline{v_\phi} \rangle_{\rm d} = & \left(\frac{H_{\rm d1}}{H} \right) \left[\frac{3}{8} V_{\rm k} \left(\frac{H}{r} \right)^2 - \frac{1}{2\Omega_{\rm k}\Sigma} \frac{\partial}{\partial r} \left(C_s^2 \Sigma \right) \right] \\ & + \left(1 - \frac{H_{\rm d1}}{H} \right) \left[-\frac{1}{2\Omega_{\rm k}\rho_{\rm o}} \frac{\partial P_{\rm o}}{\partial r} \right] \\ & - \frac{3}{8} V_{\rm k} \left(\frac{H_{\rm d1}}{r} \right)^2 + \frac{\langle \overline{v_r} \rangle_{\rm d}}{2\Omega_{\rm k} t_{\rm s*}} \end{aligned} \tag{30}$$

and

$$\begin{aligned} \langle \overline{v_r} \rangle_{\rm d} = & \left(\frac{H_{\rm d1}}{H} \right) \left[-(D - 3\nu) \frac{1}{\Sigma} \frac{\partial \Sigma}{\partial r} \right] \\ & + \left(1 - \frac{H_{\rm d1}}{H} \right) \left[-(D - 3\nu) \frac{1}{\rho_{\rm o}} \frac{\partial \rho_{\rm o}}{\partial r} - \frac{\nu_{\rm t}}{r} \frac{\partial \ln T}{\partial \ln r} \right] \\ & + 3r^{-1/2} \frac{\partial}{\partial r} \left[r^{1/2} (\nu_{\rm t} - \nu_{\rm td}) \right] \\ & + (D_{\rm d} - 3\nu_{\rm td}) \frac{1}{\Sigma_{\rm d}} \frac{\partial \Sigma_{\rm d}}{\partial r} - \frac{2\langle \overline{v_\phi} \rangle_{\rm d}}{\Omega_{\rm k} t_{\rm s*}} \end{aligned} \tag{31}$$

which are the result of interpolation between two regimes ($\Omega_{\rm k}t_{\rm s*} \rightarrow 0$ and $\Omega_{\rm k}t_{\rm s*} \rightarrow \infty$) for which the values of $\langle \overline{V_\phi} \rangle_{\rm d}$ and $\langle \overline{V_r} \rangle_{\rm d}$ have been expressed in an analytical form.

Note that the term proportional to $(D_{\rm d} - 3\nu_{\rm td})$ on the right-hand side of Eq. (31) vanishes if $K = 3$ as we have assumed. Thus, from the computational standpoint, $K = 3$ is an especially convenient case[1], and it is consistent with calculations by Canuto & Battaglia (1988). Under such an assumption, Eqs. (30), (31), and (19) combined with (10) form a closed system of equations from which $\langle \overline{v_r} \rangle_{\rm d}$, $\langle \overline{v_\phi} \rangle_{\rm d}$, and $\langle \overline{v_z} \rangle_{\rm d}$ can be calculated. The system is, in general, neither linear, nor separable because $t_{\rm s*}$ is a function of $\langle \overline{v_r} \rangle_{\rm d}$, $\langle \overline{v_\phi} \rangle_{\rm d}$, and $\langle \overline{v_z} \rangle_{\rm d}$. The solution to this system is found numerically using the relevant drag laws outlined in Paper I.

The vertical integration of the equation of continuity (1) for particles yields

$$\frac{\partial \Sigma_{\rm d}}{\partial t} + \frac{1}{r} \frac{\partial}{\partial r} \left(r \int_{-\infty}^{+\infty} \overline{\rho_{\rm d} V_{r{\rm d}}} dz \right) = 0 \tag{32}$$

and the integral under the radial partial derivative can be substituted from the vertically integrated ϕ-component of (13) to obtain

$$\begin{aligned} \frac{\partial \Sigma_{\rm d}}{\partial t} = & \frac{3}{r} \frac{\partial}{\partial r} \left[r^{1/2} \frac{\partial}{\partial r} (r^{1/2} \nu_{\rm td} \Sigma_{\rm d}) \right] \\ & + \frac{1}{r} \frac{\partial}{\partial r} \left[\frac{2r\Sigma_{\rm d} \langle \overline{v_\phi} \rangle_{\rm d}}{\Omega_{\rm k} t_{\rm s*}} \right] \end{aligned} \tag{33}$$

This equation governs the time evolution of the surface density of solid particles, $\Sigma_{\rm d}$. Parameters $\nu_{\rm td}$, $t_{\rm s*}$, and $\langle \overline{v_\phi} \rangle_{\rm d}$ depend on the size of particles and therefore are implicit functions of r, t, and $\Sigma_{\rm d}$. In order to establish these relationships we need to model the coagulation process.

3. Coagulation and evaporation processes

So far the formalism derived in Sect. 2.2 is quite similar to what we have done in Paper I, with the notable addition of the vertical analysis, which permits the evaluation of solid particles' sub-disk thickness. In a hypothetical scenario of single-sized,

[1] Note that although the condition $K = 3$ is computationally advantageous, there is nothing physically unique about it. We have also performed test calculations for $K = 1$ and have found only expected, quantitative differences between both cases.

noncoagulating, and nonevaporating particles, Eq. (33), which keeps track of radial advection and diffusion of particles, alone gives the time evolution of the surface density of solid particles. This has been done in Paper I. However, in reality, both coagulation and evaporation occur and cannot be ignored. Our method of incorporating these processes into our calculations relies on keeping Eq. (33) as the principal mathematical description of the global evolution of particles, but freeing its parameters from constraints of single-size and thermal indestructibility assumptions. Thus, our method can be characterized as solving a radial advection-diffusion problem *modulated* by coagulation, with the possibility of a cut-off by the evaporation. This method requires that the mass distribution of particles at any given radial location of a disk is narrowly peaked about a mean value particular for this location and a given time instant. Such an assumption may appear quite arbitrary; however, it has a reasonable physical justification as collisions with small particles do not significantly increase the size of a test particle and the bulk of the solid mass is concentrated in the largest, all about the same size, particles. This is supported by numerical simulations (Mizuno et al. 1988) of grain growth in protoplanetary disk which clearly show that although a broad size distribution is maintained, most of the mass is nevertheless always concentrated in the largest particles.

3.1. Coagulation

We assume that the mass distribution of particles at any given radial location r is narrowly peaked about the mean value $m_{\rm d}(r,t)$, which corresponds to the size $s(r,t)$. The goal is to evaluate the functional dependence of s on r and t. Particles are assumed to be spheres with a bulk density of ρ_s. The density of matter concentrated into solid particles is $\rho_{\rm d}(r)$ and the particles' number density is $n_{\rm d}(r)$. The geometrical cross section for collision between two such particles is $\sigma = \pi(s+s)^2$ and the mean time between collisions is $\tau_{\rm coll} = 1/(n_{\rm d}\sigma V_{\rm rel})$ where $V_{\rm rel}$ is the mean relative speed between particles. Assuming that particles stick to each other upon collision, the growth of particle mass $m_{\rm d}$ in unit time can be expressed as follow

$$\frac{dm_{\rm d}}{dt} \approx \frac{m_{\rm d}}{\tau_{\rm coll}} = \sigma\ V_{\rm rel}\ n_{\rm d}\ m_{\rm d} = 4\pi s^2\ V_{\rm rel}\ \rho_{\rm d} \tag{34}$$

To calculate $V_{\rm rel}$, we consider $\overline{\Delta V^2_{\rm d,12}} \equiv \overline{(\mathbf{V}_{\rm d,2}-\mathbf{V}_{\rm d,1})^2}$, which is the average of the square of the relative velocity between two particles at the point of collision, and we use $V_{\rm rel} = \left(\overline{\Delta V^2_{\rm d,12}}\right)^{1/2}$. Expanding $\overline{\Delta V^2_{\rm d,12}}$ we obtain

$$\overline{\Delta V^2_{\rm d,12}} = (\overline{\mathbf{V}}_{\rm d,2}-\overline{\mathbf{V}}_{\rm d,1})^2 + \overline{V'^2_{\rm d,1}} + \overline{V'^2_{\rm d,2}} - 2\overline{\mathbf{V}'_{\rm d,1}.\mathbf{V}'_{\rm d,2}} \tag{35}$$

The first term on the right-hand side of (35) corresponds to the difference between average, large-scale velocities between two particles. In our case, where both particles are assumed to have the same size, this term vanishes. The last three terms on the right-hand side of (35) stem from particles having different, chaotic, small-scale velocities at the point of collision. These terms have to be expressed in terms of large-scale quantities. It can be shown using the relations given by Cuzzi at el. (1993) that

$$\overline{V'^2_{\rm d,1}} + \overline{V'^2_{\rm d,2}} - 2\overline{\mathbf{V}'_{\rm d,1}.\mathbf{V}'_{\rm d,2}} = \frac{\overline{V'^2}}{\rm Sc_1} + \frac{\overline{V'^2}}{\rm Sc_2} - 2\frac{\overline{V'^2}}{\rm Sc_1 Sc_2} \tag{36}$$

Using (6) and (9) we can identify $\overline{V'^2}$ with $2^{1/2}R_o\alpha C_s^2$ and, if the particles are assumed to have the same size, Eq. (35) reduces to

$$V_{\rm rel}^2 = \overline{\Delta V^2_{d,12}} = 2^{3/2}R_o\alpha C_s^2\frac{\rm Sc-1}{\rm Sc^2} \tag{37}$$

which is similar to an analogical expression obtained by Morfill (1985).

Because we assume the particles to be perfect spheres, the mass of the particle is given by $m_{\rm d} = (4/3)\pi s^3\rho_s$ and Eq. (34) transforms into

$$\frac{ds}{dt} = \frac{\rho_{\rm d}}{\rho_s}\ V_{\rm rel} = \sqrt{2^{3/2}R_o\alpha}\ \frac{\rho_{\rm d}}{\rho_s}\ C_s\ \frac{\sqrt{\rm Sc-1}}{\rm Sc} \tag{38}$$

where we used (37) to eliminate $V_{\rm rel}$. Equation (38) can be integrated over the period of time equal to the time step in the solid particle's evolution [Eq. (33)] to obtain the increase of the mean particle size at any radial location of the disk. In turn, the new particle size upgrades the coefficients of Eq. (33). Continuing this process, we manage to incorporate the effects of coagulation into the global evolution of solid particles' surface density.

3.2. Evaporation

The temperature of the gas in the disk decreases with distance from the star. The particle traveling inward will evaporate when it finds itself at the location where the ambient gas is sufficiently hot. Such a location defines an evaporation radius that depends on the composition of the particle. The evaporation radius decreases with time, as the entire disk cools down in the process of its diminishment. Therefore we have to consider in our computation three instead of two components: gas, solids, and the vapor of the material constituting solid particles under cool enough conditions. As we have assumed that solid particles are made up of water ice, they cannot exist for $T > T_{\rm evap}$, and are converted into vapor. On the other hand, the vapor condenses into solid particles wherever it finds itself in a $T < T_{\rm evap}$ environment. The value of $T_{\rm evap}$ depends on parameters of the gaseous disk and thus slowly changes; however we assume that $T_{\rm evap}$ = 150 K, which is a reasonable value for all our models. In our calculations we treat vapor as particles with $s \to 0$.

3.3. Computational approach

Equation (12) is solved by means of an implicit scheme to find out the evolution of the gaseous component. The necessary opacity law is adopted according to formulas given by Ruden & Pollack (1991). The evolution of gas is computed independently from the evolution of particles (see assumptions in Sect. 1). At

every time step the quantities needed for evaluating the change in the mass distribution of solids are calculated and the change itself is computed from Eq. (33) using the operator splitting method. In such a method the advective term in (33) is treated by the numerical method of characteristics, whereas an implicit scheme is applied to the diffusion term. The obtained distribution of solid material is then modified because of the existence of the evaporation radius, and the mass distribution of the vapor is calculated using the implicit scheme. Finally, the new particle size distribution is calculated before proceeding to the next time step.

4. Global evolution of the high-mass disk

First, we applied our model to initial conditions sometimes considered fiducial by modelers of gaseous disks. The $1M_\odot$ star is surrounded by a disk with an initial gas surface density given by

$$\Sigma(r, t_o) = 8540\left[1 + \left(r/15\mathrm{AU}\right)^2\right]^{-3.78} \quad \mathrm{g\ cm^{-2}} \tag{39}$$

Thus, the initial distribution of the gas is practically constant, equal to about 8540 g cm^{-2}, between the inner radius assumed to be at 0.036 A.U. and the radius of about 15 AU. At larger distances there is practically no gas. The total mass of the gaseous disk is equal to 0.245 $M_\odot$ and angular momentum is equal to 5.6×10^{52} g cm^2 s^{-1}. In such a disk a relatively large amount of the gas is concentrated relatively close to the star; therefore, we call it a high-mass, high-concentration scenario. These initial conditions correspond closely to the "standard case" considered by Ruden & Pollack (1991) and are identical to those we have used in Paper I. We further assume that the dimensional viscosity parameter α is equal to 10^{-2}, the fiducial value assuming that the disk's turbulence is driven by thermal convection.

Of course, the assumed initial surface density profile is arbitrary. Fortunately, the specific form of the profile does not influence the subsequent evolution of the gas, inasmuch as the process governed by Eq. (12) is diffusive in nature and the details of initial distribution are forgotten after a time short in comparison with the evolutionary timescale. Taking advantage of the "short memory" of the gaseous component, we introduce solid particles into the calculation only after the passage of 10^4 yr during which the gas evolves alone to get rid of the arbitrariness in the initial condition. Upon introduction, the solid particles all have the same size, $s = 10^{-3}$ cm, and the surface density of the solid material constitutes 1% of the contemporaneous gas surface density to account for cosmic abundance.

The calculations are carried out for up to $t = 3.2 \times 10^6$ yr, a period of time equal, within an order of magnitude, to observationally deduced lifetimes of protoplanetary disks (Strom & Edwards 1993). Fig. 1 shows the summary of the disk evolution starting from the high-mass initial conditions described above. The design of Fig. 1, as well as the design of subsequent figures in Sect. 5, is the following: panel (a) shows the evolution of Σ, panel (b) shows the evolution of Σ_d, panel (c) shows the changes in s, panel (d) shows the changes in H_d, and panel (e) shows the

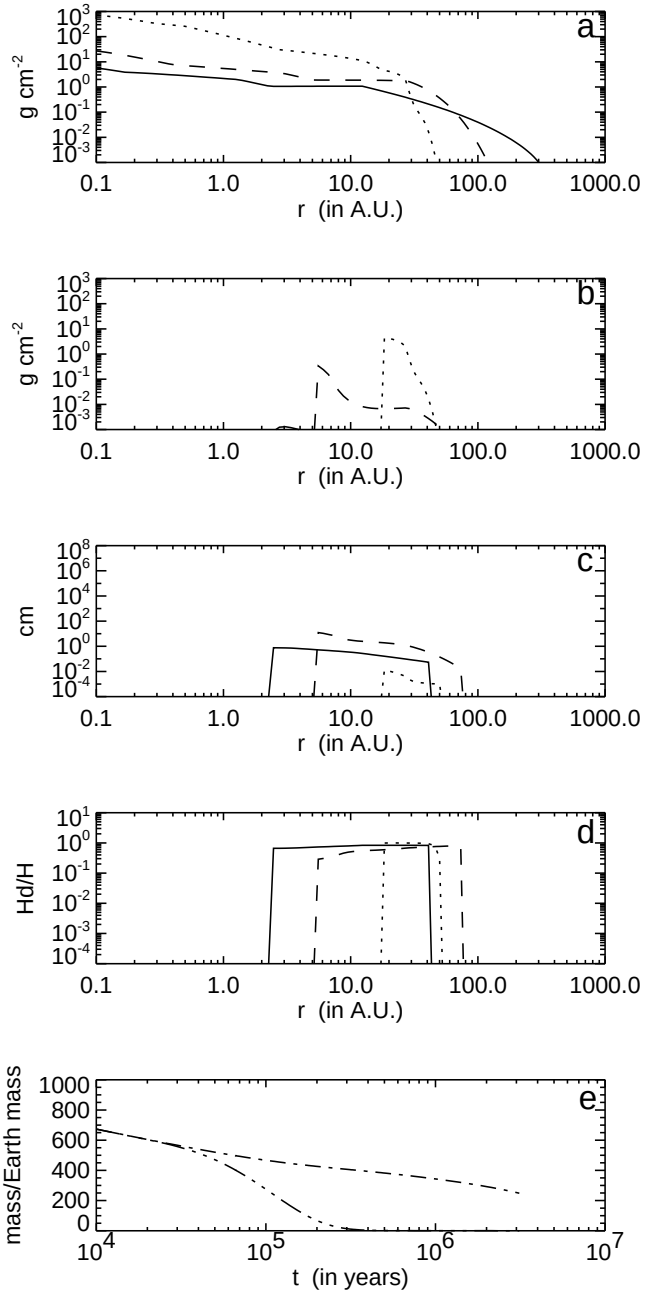

Fig. 1a–e. Summary of the evolution of gas and solids for the high-mass initial conditions scenario with $\alpha = 10^{-2}$. Panels **a** to **d** show the surface density of the gas, Σ; the surface density of solid particles, Σ_d; the particle size, s; and the thickness of solids sub-disk, H_d, respectively, as functions of r at selected times. On panel (a) the values of Σ are divided by a factor of 10^2 to put it in the same order of magnitude as Σ_d. Various times are labeled by different line styles: the dotted line denotes $t = 10^4$ yr, the dashed line denotes $t = 3.2 \times 10^5$ yr, and the solid line denotes $t = 3.2 \times 10^6$ yr. The time elapses from the moment when solid particles are introduced into the disk. Panel **e** shows the time evolution of the total mass of the disk, the dash-dot line represents the mass of the gaseous disk divided by a factor of 10^2, and the dash-dot-dot-dot line represents the mass of the solids sub-disk.

evolution of the total mass of both gaseous and solid, components of the disk. Although these quantities are calculated and available at any given time during the evolution of the disk, the figures show only three snapshots: at $t = 10^4$ yr, or at the very beginning of the evolution; at $t = 3.2 \times 10^5$ yr, or at the midway of particle evolution; and at $t = 3.2 \times 10^6$ yr, when the surface density of solids has converged.

The most important result of the high-mass model calculation is that such a model leads to a complete loss of all solids into the star. This can be seen from panels (b) and (e) on Fig. 1. A failure of this seemingly reasonable model to lock any solids into bodies that can permanently orbit the star is somehow disappointing, but readily understandable from concomitant actions of the processes occurring in a disk. The disk evolving from the high-mass initial conditions remains relatively hot for a long time. Therefore the ice/vapor interface is located beyond 10 A.U. for up to 10^5 yr. However, on a timescale of only 10^4 yr, particles located beyond this interface coagulate to sizes of the order of 1–10 cm, decouple from the gas, and start moving inward. Their inward movement is swift (see Paper I for details) and the distance to the evaporation radius is short, so particles have no time to further grow by coagulation and thus stop their motion toward the destruction zone. The end result is that particles never grow to sizes bigger than about 10 cm (see Fig. 1c), and eventually they are all destroyed, leaving a purely gaseous disk behind (see Fig. 1b). Note that because particles have no chance to grow to larger sizes, they remain quite well coupled to the turbulent eddies (but not to the large-scale motion of the gas), and therefore are distributed throughout the entire thickness of the disk, so $H_{\rm d}$ always remains comparable to H (see Fig. 1d).

A disk evolving from the high-mass initial conditions does not lead to the formation of planetesimals. Two features of this model, its high surface density and compactness, are responsible for destruction of all solids. The high surface density translates into the high temperature and the outward location of the evaporation radius. The compactness of the disk translates into a short distance between the outer edge of the disk and the evaporation radius. Once particles grow to the size of maximum radial velocity (1–10 cm, see Paper I), their travel time to the evaporation radius is shorter than the characteristic coagulation time.

5. Global evolution of the low-mass disk

In order to produce planetesimals the initial disk must apparently be less massive and more extended than the one considered in the previous section. Therefore we consider a scenario where the $1M_\odot$ star is surrounded by a disk with the initial surface density of the gas given by

$$\Sigma(r,t_{\rm o}) = 2\Big[1+\big(r/200{\rm AU}\big)^2\Big]^{-3.78} + 600\big(r/1{\rm AU}\big)^{-1.5} \ {\rm g\ cm^{-2}} \qquad (40)$$

The first term ensures that there is some mass up to very large distances from the star. The second term corresponds to the central concentration of the mass and sets the location of the evaporation radius. The total mass of the gaseous disk is equal to 0.023 $M_\odot$ and an angular momentum is equal to 1.8×10^{52} g cm^2 s^{-1}. Overall, the disk described by this model has about an order of magnitude less mass than the disk described by the previous model; therefore, we call it a low-mass scenario. Our calculations, starting from the low-mass initial conditions, are carried out identically to those started from the high-mass initial conditions. Figs. 2, 3, 4, and 5 summarize the low-mass disk evolution for values of dimensional viscosity parameter α equal to 10^{-1}, 10^{-2}, 10^{-3}, and 10^{-4} respectively. This range covers all values of α that are conceivable in the context of protoplanetary disks.

The most important result of the low-mass model calculation is that such a model leads to the survival of solid material. This manifests itself by the emergence of the *converged*, nonvanishing surface density distribution of solids (panel (b) of Figs. 2–5). It is interesting that although the converged radial distribution of the solid material depends on the value of α, the total mass of solids in a disk is about the same, independent of the value of α, and approximately equal to the initial mass of solids in the disk (panel (e) of Figs. 2-5). Thus, the evolution of the low-mass disk results in the reshuffle of solids within the disk, but not to their loss into the star. Of course, some solids, those initially located close to the evaporation radius, are lost, but, given the initial mass distribution (40), they constitute a small percentage of the total solid material, which is predominantly located in the outer disk. Once particles in the outer disk grow to the size of maximum radial velocity, their characteristic travel time to the evaporation radius is longer than the characteristic coagulation time so they manage to stop their radial movement before reaching the destruction zone.

The value of α determines the radial distribution of solids: the smaller the value of α, the broader the distribution of solids. This is because particles suspended in a more vigorously turbulent disk (larger value of α) have larger inward radial velocities and consequently are locked into planetesimals closer to the star than particles in a less turbulent disk. The evaporation radius is located between 1 AU and 2 AU for all values of α, the outer limit of converged $\Sigma_{\rm d}$ is about 10 AU for $\alpha = 10^{-1}$ and $\alpha = 10^{-2}$, about 30 AU for $\alpha = 10^{-3}$, and about 60 AU for $\alpha = 10^{-4}$.

By the time the surface density of solids attains convergence, the particles coagulate to about 10^6 cm, or planetesimal sizes (panel (c) Figs. 2-5). In disks characterized by smaller values of α, and thus a more extended distribution of solids, the range of sizes, from 10^6 cm at the evaporation radius to 10^4 cm at the outer limit, can be found. This is because the coagulation process is less efficient at larger radii. These solids will continue to increase their sizes, but will not change their radial position, as they are already large enough to have a negligible radial motion. The thickness of the solid particles sub-disk, given by Eq. (21) depends both on the particle size and on the value of α. Examining panels (d) of Figs. 2-5, it can be seen that the smaller the value of α, the relatively thinner the particle sub-disk. This is intuitively easy to understand, as a more turbulent (larger

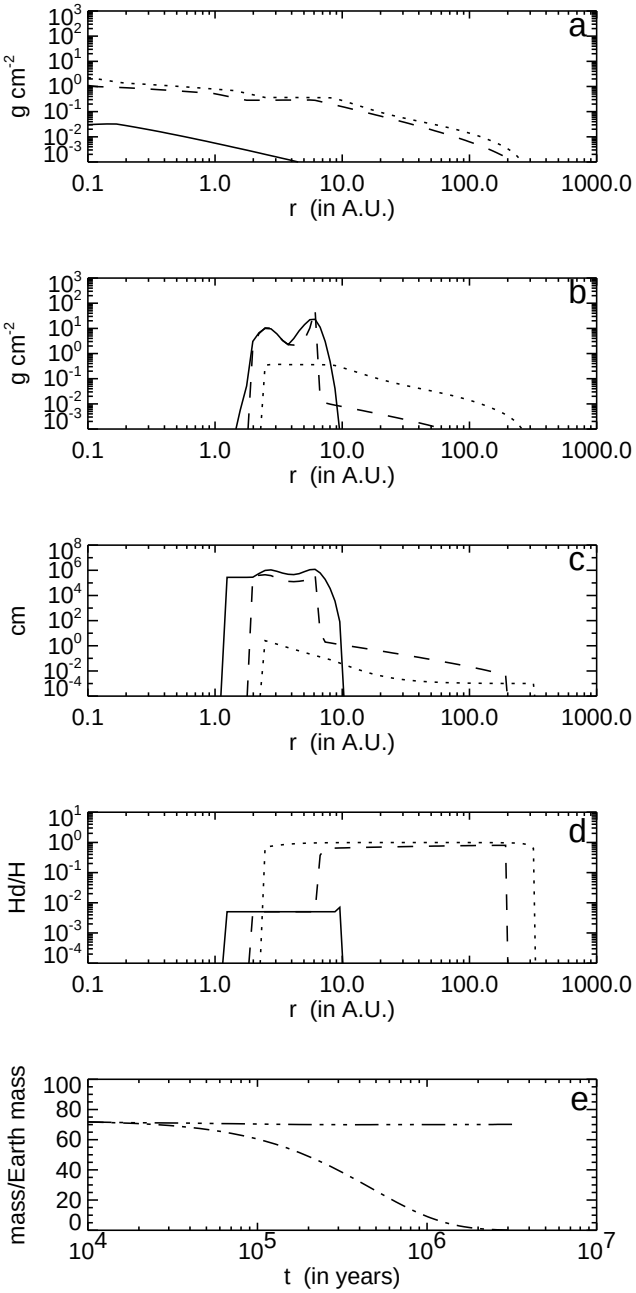

Fig. 2a–e. Summary of the evolution of gas and solids for the low-mass initial conditions scenario with $\alpha = 10^{-1}$. See Fig. 1 for legend.

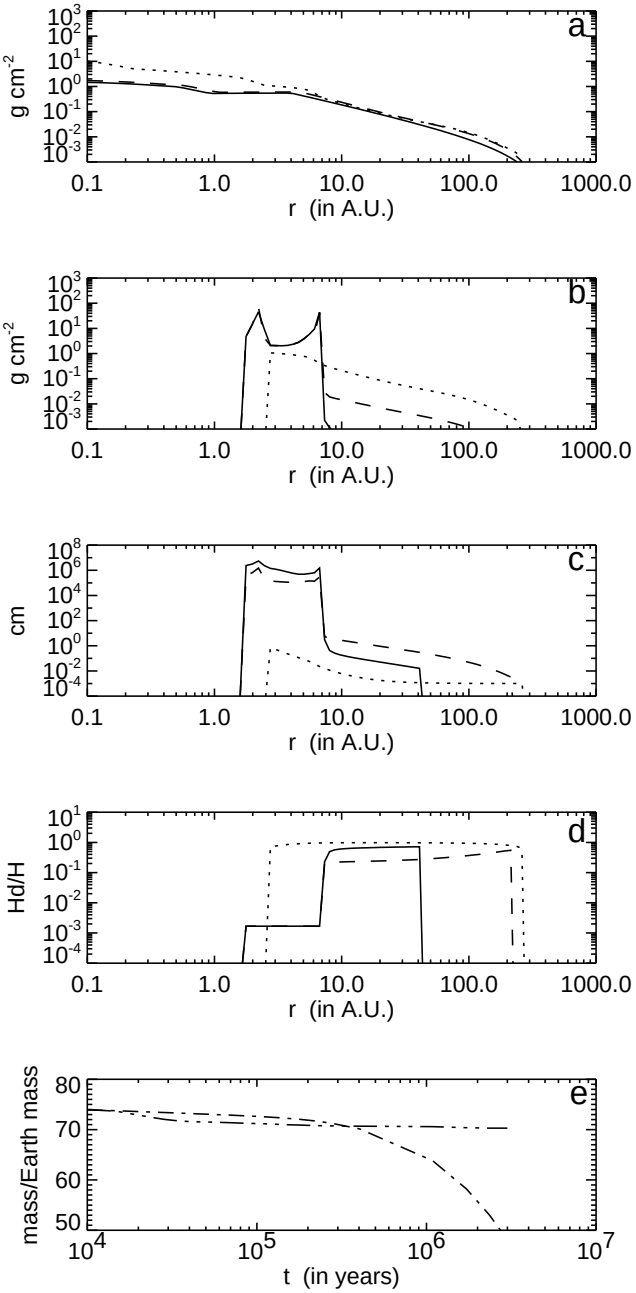

Fig. 3a–e. Summary of the evolution of gas and solids for the low-mass initial conditions scenario with $\alpha = 10^{-2}$. See Fig. 1 for legend.

value of α) disk inhibits sedimentation of particles. In any case, by the time the surface density of solids attains convergence, the particles form a layer 10^{-2}–10^{-4} times thinner than the surrounding gaseous disk.

Note that the converged radial distribution of solids does not vary monotonically. There are bulges of matter near the evaporation radius as well as at the outer limit of $\Sigma_{\rm d}$. These bulges are present in all cases, but become narrower for smaller values of α. Their existence is a consequence of an intricate and nonlinear interdependence between advection and coagulation, modulated by changing gas conditions and the character of turbulence (the value of α).

Consider the region outside the evaporation radius, $r_{\rm evap}$. The efficiency of coagulation is a decreasing function of the radius [see Eq. (38)] so, shortly after evolution starts, the particle size is also a decreasing function of the radius. As particles grow they acquire inward radial velocities in excess of the gas inflow velocity. There exists a particular size, $s_{\rm f} = 1-10$ cm, for which the radial velocity of a particle is fastest. For as long as the particles near the evaporation radius are all smaller than $s_{\rm f}$, the

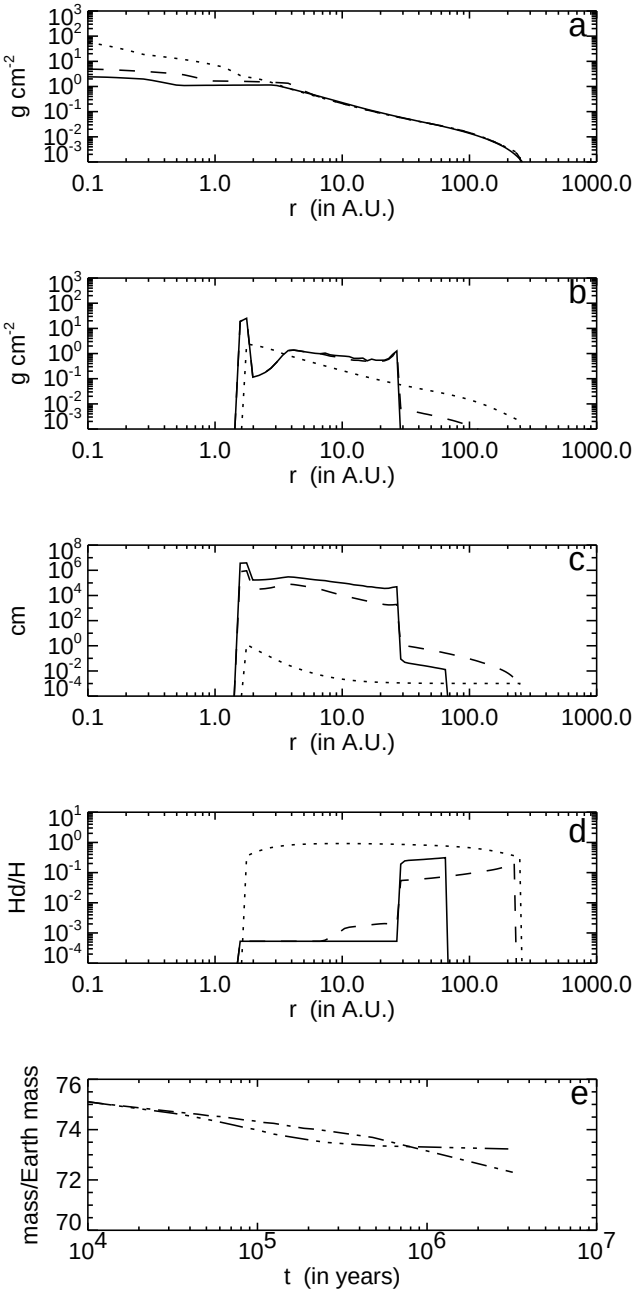

Fig. 4a–e. Summary of the evolution of gas and solids for the low-mass initial conditions scenario with $\alpha = 10^{-3}$. See Fig. 1 for legend

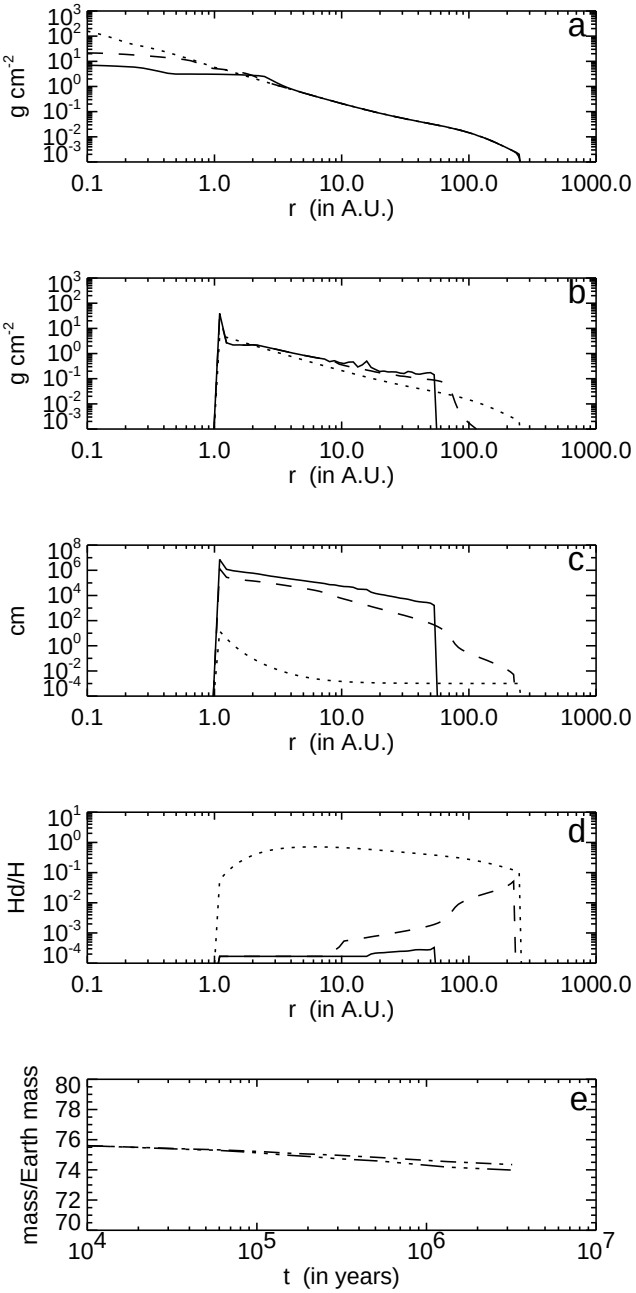

Fig. 5a–e. Summary of the evolution of gas and solids for the low-mass initial conditions scenario with $\alpha = 10^{-4}$. See Fig. 1 for legend.

coagulation rate is actually impeded as the density of particles decreases due to monotonically decreasing advection velocity. Particles pass $r_{\rm evap}$ and are lost. This process will continue, and may, as in the case of the scenario considered in Sect. 4, bleed the disk of all solids, unless particles bigger than $s_{\rm f}$ start arriving at $r_{\rm evap}$. For this to occur, the disk must be large enough. With the appearance of particles larger than $s_{\rm f}$, an advection velocity is no longer monotonically decreasing; instead, particles at $r_{\rm evap}$ move slower than more remote particles, which leads to a fast increase of particle density at $r_{\rm evap}$ and corresponding increase in the coagulation rate. The two phenomena, increasing density and enhanced coagulation rate, form a self-feeding loop resulting in a very rapid growth of particles and formation of the bulge in the solids surface density near $r_{\rm evap}$. The formation of this bulge also signals the "freezing" of the total mass of the solids in the disk, inasmuch as no more solids are lost to the vapor zone in subsequent disk evolution. They will either be captured by the bulge or come to rest by themselves at larger radii. Notice that it is a radial squeezing due to particle dynamics, rather than vertical squeezing due to sedimentation, that is primarily

responsible for establishing the bulge and keeping particles from falling into the vapor zone.

The same mechanism is responsible for the abrupt drop in $\Sigma_{\rm d}$, which we associate with the outer limit of solid matter distribution, as well as the presence of the $\Sigma_{\rm d}$ bulge at the location of this drop. The outer region of the disk is characterized by the slowest coagulation rate, so particles there can travel relatively long distances before acquiring a size larger than $s_{\rm f}$. Once they grow to $s > s_{\rm f}$, they slow down, allowing particles that trail them to catch up and form the bulge in the fashion described above. With time, the entire region beyond the outer bulge is swept clean of particles.

6. Discussion

In this paper we have studied the global evolution of solids in protoplanetary disks. We have demonstrated that it is possible, under certain assumptions, to approach the problem of how a planet-building material is spatially distributed, from physical principles rather than phenomenologically, like in the minimum-mass solar nebula model (Hayashi et al. 1985). The basic problem is as follows: given some initial state, presumably chosen to reflect conditions at the onset of protoplanetary disk evolution, what is the spatial distribution of solids after they accumulate into planetesimals? On that issue, and under assumptions stated in Sect. 1, we have obtained the following results.

(1) The outcome is sensitive to the assumed initial conditions. The shape of the initial distribution of the gas and dust around the star makes a big difference in the ultimate location of the planetesimal swarm. Moreover, it is plausible, and has been demonstrated in Sect. 4, that some, otherwise perfectly reasonable, initial distributions of matter, lead to the extinction of all solid material from the disk. Therefore our results seem to contradict the widespread but unsubstantiated believe that planetary systems are the natural and unavoidable product of the star formation process. Instead, it appears that whether or not solid planetary cores can emerge from the star formation process depends on how this formation process proceeds. If the viscous stage starts from a relatively compact disk, solids are lost and no solar-system-like planets could form. If, on the other hand, the viscous stage begins with the disk extending up to large distances from the star, solid planetesimals, and subsequently planets/cores will develop. We may point out that observations of T Tauri stars (for a review, see Strom & Edwards 1993) suggest the existence of extended disks that, according to our calculations, are likely to form planetesimals. However, it remains uncertain whether these disks reflect the condition of a circumstellar material at the onset of the viscous stage, or rather during this stage after the original disk spread significantly.

(2) Of four basic processes governing the evolution of solids, advection, coagulation, sedimentation, and evaporation, the interplay between the first two is the single most important factor in determining the outcome. Advection draws solids toward the star, and coagulation first enhances, then inhibits, and ultimately stops the advection. The fate of particles is decided by the race between advection and coagulation. Sedimentation helps increase the coagulation rate, but is superseded in importance by advectional compression at the crucial stage of the inner bulge formation. Evaporation sets the inner limit of the distribution of planetesimals. Since there is a bulge in the number density of planetesimals at the location of the evaporation radius, one can speculate that the location of the innermost planet (in our case the innermost icy planet or the planet with the icy core) is determined by the evaporation radius.

(3) If the extended initial mass distribution is assumed (like the one considered in Sect. 5) solids evolve into planetesimals. After times shorter than 3.2×10^6 yr the radial distribution of planetesimals' number density settles and can only change on a much longer timescale by processes not considered in our model [like mutual gravitational interactions between planetesimals proposed first by Safronov (1968)]. Note that $\sim 10^6$ yr is the time required for $\Sigma_{\rm d}$ to converge *everywhere*; however, this convergence is not uniform and can be achieved on a time scale as short as 10^4 yr in the innermost disk. The radial extent of the planetesimal swarm depends on the assumed value of α, but the total mass of the swarm does not. In fact, the final mass of solid material locked into planetesimals is about equal to the initial mass of solids distributed among all 10^{-3} cm particles. That means that the total mass of the solid constituent of planets is fixed by the mass of dust in the initial disk. Regardless of the value of α, the number density of planetesimals has an abrupt outer limit resulting from advectional compression. This leads to the prediction that planetary systems end abruptly. This is certainly true of our solar system, where the mass of all objects in the Kuiper belt is estimated to be only a fraction of Earth's mass (Jewitt & Luu 1995).

We believe that our model captures the essence of processes leading to the distribution of icy planetesimals. There are certain assumptions in our model that reflect the present-day state of knowledge on the topic of protoplanetary disks, and, if revised, can change our conclusions. Most importantly, we envision that the protoplanetary disk indeed undergoes *viscous* evolution, and it is during that viscous stage, which is further assumed not to be accompanied by any infall of material, that the evolution of solids take place. Furthermore, we model the viscous disk to be powered by uniform turbulence, characterized by a constant value of α. In principle, our method does not depend on the fact that the underlying gaseous disk is described by a viscous model. We can, as well, couple the solid component to the gaseous component powered by a different mechanism (for example, magnetic torque), although such a disk should still be turbulent, because it is turbulence that makes coagulation possible in our model. In addition, we assume that small solid particles are initially homogeneously distributed throughout the gas, changing this assumption may produce different results.

Within these assumptions, we have made a number of approximations. We believe that important aspects of our results are not artifacts of these approximations. Following Cuzzi et al. (1993) we consider the protoplanetary disk as a two-phase fluid flow, the mixture of the gas and the "fluid" of solid particles. The fluid approximation is valid for small ($\Omega_{\rm k} t_{\rm s*} \rightarrow 0$) particles because of their strong coupling to the gas, and for large

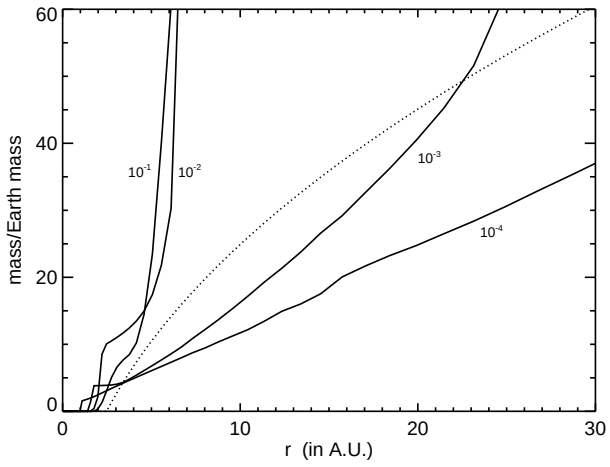

Fig. 6. The plot of the disk's mass interior to a given radius versus the radius for different solid mass distributions. Solid lines represent mass distributions calculated starting from the low-mass initial conditions. Different solid lines are labeled by the value of α. The dotted line represents the mass distribution of the icy solid material in the solar system spread over the outer solar system according to the minimum-mass model.

($\Omega_{\rm k} t_{\rm s*} \rightarrow \infty$) particles because they move on near-keplerian orbits in the midplane thus constituting a "cold," two-dimensional fluid. The motion of intermediate-sized ($\Omega_{\rm k} t_{\rm s*} \sim 1$) particles cannot be consider two-dimensional as they undergo damped vertical oscillations around the midplane (Nakagawa et al. 1986). For such particles the fluid description may not be fitting for their behavior in the vertical direction. Nevertheless, as the characteristic decay time for intermediate-sized particles oscillations is short (of the order of ${\Omega_{\rm k}}^{-1}$), the thickness of the particle subdisk is primarily controlled by turbulent diffusion and should not be strongly influenced by oscillations of individual particles. Overall, we feel that the fluid approach provides at least a qualitatively correct description of solid particles in the protoplanetary disk.

The approximation that the mass distribution of particles is narrowly peaked about the mean value artificially decreases the rate of coagulation because particles having the same size can coagulate only due to the difference in turbulent speed, and not the difference in the systematic speed stemming from particles having different sizes. However, for our purpose, only mechanisms leading to the growth of the largest particles, the ones that contain the bulk of the mass, are important. The encounters of these particles with the small particles, due to the difference in their regular velocities, does not increase the size of the large particle significantly. On the other hand, encounters between two large particles, due to the difference in their turbulent speeds, increase the size of the particle significantly. Thus, our approximation should give a coagulation rate of the right magnitude, which is the only accuracy we are seeking at this stage.

Our assumption of the perfect sticking coefficient assures the formation of planetesimals. In reality, sticking coefficient depends on the relative velocity between particles. However, because the bulk of the solid mass is concentrated in the largest, all about the same size, particles, the perfect sticking coefficient is a reasonable assumption for our purpose of studying the global evolution of solid mass, as the relative velocity between particles of the same size is minimized. Other approximations, such as ice-only solids, and neglecting the feedback of the solid component on the gaseous component have obviously only a minor effect on our results. The addition of other components of solids, such as "rock" and "metal" will not introduce any new insights in to the problem, although it would permit consideration of planetesimals closer to the star, for modeling the "terrestrial" zone.

Finally, we assess how the distribution of the solid mass calculated in Sect. 5 compares to that found in our solar system. Of course, we don't know what was the distribution of planetesimals in the solar nebula, we only know the present locations and masses of planets. From this data it is customary to "reproduce" the continuous surface density of solids. According to Hayashi et al. (1985) such a surface density of icy solids in the solar nebula has the form

$$\Sigma_{\rm d}^{\rm ss} = 30 \Big(\frac{r}{\rm AU} \Big)^{-3/2} \quad {\rm g\ cm}^{-2} \tag{41}$$

This distribution extends from 2.7 AU (evaporation radius) to 36 AU. It is convenient to consider the mass of the disk interior to a given radius

$$M_{\rm d}^{\rm ss}(r) = \int_{r_{\rm in}}^{r} 2\pi x \Sigma_{\rm d}^{\rm ss} dx \tag{42}$$

The dotted line on Fig. 6 shows $M_{\rm d}^{\rm ss}(r)$. Our low-mass model yields $\Sigma_{\rm d}$ and we can calculate $M_{\rm d}(r)$, which is represented on Fig. 6 by the solid line. Note that all models have similar total mass with our models having a little higher mass than Hayashi's model. At first, it seems that our models cannot yield a solar-system-like configuration. Indeed, mass distribution in models characterized by $\alpha = 10^{-1}$ and $\alpha = 10^{-2}$ do not extend far enough to account for the architecture of the solar system, and the mass distribution in the model characterized by $\alpha = 10^{-4}$ does not have enough mass within the inner 30 AU. Only mass distribution in the model characterized by $\alpha = 10^{-3}$ has the mass and almost the extension to account for the solar system, but its mass distribution $M_{\rm d}(r)$ is markedly different from $M_{\rm d}^{\rm ss}(r)$. However, it is important to remember that $M_{\rm d}^{\rm ss}(r)$ is an artificially constructed quantity, and as such is only one of many mass distributions from which planetary masses and locations can be produced. Assume that four giant planets in the solar system have cores of $M_{\rm J} = 20 M_\oplus$, $M_{\rm S} = 20 M_\oplus$, $M_{\rm U} = 10 M_\oplus$, and $M_{\rm N} = 10 M_\oplus$ respectively. From Fig. 6 we can find out that, according to $M_{\rm d}^{\rm ss}$, the mass constituting the core of Jupiter comes from the zone between 2.7AU and 8.3AU, the mass constituting the core of Saturn comes from the zone between 8.3AU and 16.8AU, the mass constituting the core of Uranus comes from the zone between 16.8AU and 23AU, and the mass constituting the core of Neptune comes from the zone between 23AU

and 30AU. The phenomenological model has been constructed in such a fashion that the location of planets are obtained by taking the geometric average of the outer and the inner limit of the corresponding zone. This gives, $r_{\rm J}$ = 4.7AU, $r_{\rm S}$ = 11.8AU, $r_{\rm U}$ = 19.6AU, and $r_{\rm N}$ = 26AU. These location are not exactly where the planets actually are because Hayashi's model assumes different values for masses of the giant planets cores. Applying the same procedure to our $\alpha = 10^{-3}$ model we obtain "solar giant planets" at locations, $r_{\rm J}$ = 4.05AU, $r_{\rm S}$ = 15AU, $r_{\rm U}$ = 21AU, and $r_{\rm N}$ = 23.6AU, which in these qualitative terms is not much different from the actual locations. The most important difference is the excess of mass near the outer limit of the mass distribution. This causes "Neptune" to be too close to "Uranus." Keeping in mind that our model starts from arbitrary initial conditions and is not expected to actually reproduce the solar system, the excess of mass at 20–30 AU may nevertheless account for the mass lost from the plane of the ecliptic due to gravitational scattering of unaccreted planetesimals by planets that have already attained their final masses (Duncan et al. 1987). Overall, our model seems to account quite well for the large-scale character of our solar system while clearly indicating that planetary systems of different layouts are possible.

Acknowledgements. This research was done while the authors were supported by the Lunar and Planetary Institute, which is operated by USRA under contract No. NASW-4574 with NASA. This is Lunar and Planetary Institute Contribution No. 897.

References

Canuto, V.M. & Battaglia, A. 1988, A&A, 193, 313
Cuzzi, J.N., Dobrovolskis, A.R., Champney, J.M. 1993, Icarus, 106, 102
Dubrulle, B., Morfill, G., Starzik, M. 1995, Icarus, 114, 237
Duncan, M., Quinn, T., Tremaine, S. 1987, AJ, 94, 1330
Hayashi, C., Nakazawa, K., Nakagawa, Y. 1985, in Protostars & Planets II, ed. D.C. Black & M.S. Matthews (Univ. of Arizona Press, Tucson), 1100
Jewitt, D.C., Luu, J.X., AJ, 1995, 109, 1867
Mayor, M., Queloz, D. 1995, Nature, 378, 355
Mizuno, H., Markiewicz, W.J., Völk, H.J. 1988, A&A, 195, 183
Morfill, G.E. 1985, in Birth and Infancy of Stars, ed. R. Lucas, A. Omont & R. Stora (Elsevier Science Publishers), 693
Nakagawa, Y., Sekiya, M., Hayashi, C. 1986, Icarus, 67, 375
Ruden, S.P., Pollack, J.B. 1991, ApJ, 375, 740
Safranov, V.S. 1968, in: Evolution of the Protoplanetary Cloud and the Formation of the Earth and Planets (Nauka Press, Moscow)
Stepinski, T.F., Valageas, P. 1996 A&A, 309, 301
Strom, S.E., Edwards, S. 1993, in: Planets around Pulsars, ed. J.A. Phillips, S.E. Thorsett & S.R. Kulkarni (ASP Conf. Ser., 36), 235
Weidenschilling, S.J., Cuzzi, J.N. 1993, in Protostars & Planets III, ed. E.H. Levy & J.I. Lunine (Univ. of Arizona Press, Tucson), 1031

This article was processed by the author using Springer-Verlag LaTeX A&A style file *L-AA* version 3.